A Miniaturized Ultrasonic Micro-hole Perforator for Minimally Invasive Craniotomy

Shufu Liao#, Xuan Li#, Maosen Deng, Bin Liu, Yatong Wang, Shier Nee Saw, Zhe Li*

Abstract—*Objective:* **Micro-hole perforation on skull is urgently desired for minimally invasive insertion of micro-tools in brain for diagnostic or treatment purpose. However, a micro drill bit would easily fracture, making it difficult to safely generate a micro-hole on the hard skull.** *Methods:* **In this study, we present a method for ultrasonic vibration assisted micro-hole perforation on skull in a manner similar to subcutaneous injection on soft tissue. For this purpose, a high amplitude miniaturized ultrasonic tool with a 500 μm tip diameter micro-hole perforator was developed with simulation and experimental characterization. In-depth investigation of micro-hole generation mechanism was performed with systematic experiments on animal skull with a bespoke test rig; effects of vibration amplitude and feed rate on hole forming characteristics were systematically studied. It was observed that by exploiting skull bone's unique structural and material properties, the ultrasonic micro-perforator could locally damage bone tissue with micro-porosities, induce sufficient plastic deformation to bone tissue around the micro-hole and refrain elastic recovery after tool withdraw, generating a micro-hole on skull without material.** *Results:* **Under optimized conditions, high quality micro-holes could be formed on the hard skull with a force (< 1N) even smaller than that for subcutaneous injection on soft skin.** *Conclusion:* **This study would provide a safe and effective method and a miniaturized device for micro-hole perforation on skull for minimally invasive neural interventions.**

Index Terms—Ultrasonic vibration, bio-manufacturing, skull bone, craniotomy, micro-hole forming, bio-composite

Shufu Liao, Maosen Deng, Yatong Wang, and Zhe Li are with Guangdong Provincial Key Laboratory of Sensor Technology and Biomedical Instrument, School of Biomedical Engineering, Sun Yat-Sen University, Guangzhou 510006, China; School of Biomedical Engineering, Shenzhen Campus of Sun Yat-sen University, Shenzhen 518107, China (e-mail: liaoshf@mail2.sysu.edu.cn; hnxydms@163.com; wangyt59@mail2.sysu.edu.cn; lizhe28@mail.sysu.edu.cn).

Xuan Li is with Centre for Medical and Industrial Ultrasonics, James Watt School of Engineering, University of Glasgow, Glasgow G12 8QQ, U.K (e-mail: xuan.li@glasgow.ac.uk).

Bin Liu is with International School of Information Science & Engineering, Dalian University of Technology, Dalian 116024, P.R. China (e-mail: liubin@dlut.edu.cn).

Shier Nee Saw is with Department of Artificial Intelligence, Faculty of Computer Science and Information Technology, Universiti Malaya, 50603, Kuala Lumpur, Malaysia (e-mail: sawsn@um.edu.my).

# These authors contribute equally to the work.

I. INTRODUCTION

IN minimally invasive neural intervention, micro-tools such as micro-electrodes or micro-catheters need to be inserted in brain for treatment of diagnostic purpose such as targeted drug delivery, tumor tissue biopsy or localized neuromodulation [1-4]. However, as brain is protected by skull, a high strength bio-composite material with micro-porosities, this natural barrier needs to be penetrated for the insertion of micro-tools for minimally invasive neural intervention. Perforation of skull bone is conventionally achieved by material-removal techniques such as drilling/grinding [5, 6]. Due to the high strength of skull bone (Young's modulus of 22-45 GPa [7]), a micro drill bit would easily fracture under a large thrust force, making it difficult to safely generate a micro-hole on skull by drilling. Meanwhile, as bone tissue is removed by rotating cutting edges in the conventional drilling craniotomy, rotating cutting edges would pose a great thread to soft tissue such as dura or even brain tissue at the end of skull perforation [5].

To address this issue, low frequency or ultrasonic vibration has been incorporated to change the tool-tissue interaction. Alam et al. demonstrated that ultrasonic vibration could effectively reduce the thrust force, but displacement amplitude was found to have minimal effects on the drilling force [8]. Li et al. developed an information feedback self-adaptive harmony search algorithm to minimize the thrust force in bone drilling [9], showing that low frequency vibration (≤ 1 kHz) was also effective in reducing the thrust force under optimized parameters. Despite the advances in vibration assisted manufacturing, micro-hole drilling on skull for minimally invasive neural intervention was rarely reported. Meanwhile, researchers also investigated the possibility of laser drilling on bone [10-12]. However, it is difficult to accurately monitor the laser drilling terminal in physiological conditions and over-cutting would cause serious damage to brain tissue [10]. Due to the lack of safe techniques for micro-hole craniotomy, insertion of micro-tools in brain is conventionally conducted through a large burr hole opened on skull, leading to serious tissue damage and cerebrospinal fluid leakage which may cause

brain shift [13] and impair implantation accuracy of the micro-tool for neural intervention [14].

Different from soft tissue such as abdominal skin which can be easily penetrated by a syringe needle, skull bone is a high strength bio-composite material composed of organic collagen fibers and inorganic hydroxyapatite components [7, 15] and it is hard to be penetrated by a slender micro-tool which would bend or fracture during indentation. Meanwhile, skull bone is microscopically porous with a porosity of 5-10% for the cortical bone and 70-95% for the sponge bone; this porous structure can be compressed and plastically deformed under loading [15-17]. In response to urgent need for micro-hole perforation on skull in minimally invasive neural operations, this study presents a novel method for micro-hole perforation on skull with a miniaturized micro-hole perforator.

In this article, inspired by acupuncture and subcutaneous injection on soft tissue, a miniaturized ultrasonic device with a conically tipped micro-perforator (500 μm diameter) was developed in this study to enable micro-hole formation on the hard skull. Rational design of the miniaturized ultrasonic micro-perforator was performed with simulation and experimental characterization. Systematic experiments were conducted on animal skull to investigate micro-hole formation mechanism by comparing the thrust force, diameter and morphology of micro-holes generated under different vibration amplitudes and feed rates. With the assistance of high amplitude ultrasonic vibration, the conically tipped micro-perforator could microscopically damage skull bone's micro-porous structure, plastically deform and squeeze bone tissue around the conical tip, presenting a novel method for micro-hole forming on skull. Under optimized conditions, high quality micro-hole formation on skull has been achieved with a force (< 1 N) even smaller than that for soft tissue (porcine skin) penetration by a subcutaneous injection needle, showing its great potential for applications in minimally invasive neural operations.

II. DEVICE DEVELOPMENT

A. Vibration Mode Analysis of Piezoelectric Rings

In order to design a high performance ultrasonic micro-hole perforator, electromechanical properties of the piezoelectric rings should be investigated. Lead zirconate titanate (PZT) piezoelectric rings from the same batch were used to ensure consistency of material properties (PIC-181, PI Ceramic; outer diameter: 10 mm; inner diameter: 5 mm; thickness: 2 mm). Electrical characteristics of the piezoelectric ring were measured using an impedance spectrum analyzer (4294A, Agilent) with a swept signal of 1.0 V (peak-to-peak).

Fig. 1(a) shows the electrical impedance and phase characteristics of the PIC181 ring. Three distinctive peaks could be detected in the frequency range of 10 kHz to 1 MHz, which are denoted as A, B and C, respectively, representing three vibration modes of the piezoelectric ring. Frequency response characteristics (calculated as the average velocity on the surface of the PIC181 ring) for different vibration modes

are compared in Fig. 1(b). As for Mode A, it would represent the radial mode of the piezoelectric ring; its velocities in X and Y directions are similar, which are considerably higher than that in the Z direction, confirming the dominant radial motion. As for Mode C, the velocities in all directions have similar amplitudes; inner and outer edges of the piezoelectric ring are moving up and down in-phase, while the central region of the ring surface stays almost static. In Mode B, the velocity in the thickness direction (or the Z direction) exhibits the largest amplitude; this mode is recognized as piezoelectric ring's thickness mode.

To identify the vibration mode shapes, finite element analysis (FEA) was performed using Abaqus-Simulia (Dassault Systèmes, Vélizy-Villacoublay, France), which was validated by experimental modal analysis (EMA) with a MSA-100 3D Laser Doppler Vibrometer (Polytec, Waldbronn, Germany). Fig. 1(c) compares the three vibration modes predicted in FEA and measured in EMA. Based on the FEA and EMA results, the miniaturized ultrasonic micro-hole perforator will be developed based on the thickness mode of the piezoelectric ring (or Mode B in Fig. 1(c-2)). Also, as shown in Fig. 1(c-2), there is a good agreement between the FEA predictions and the EMA measurements in terms of deformation and resonance frequency; this accurate and reliable FEA model of piezoelectric rings will be used for the design of the miniaturized ultrasonic tool in the following.
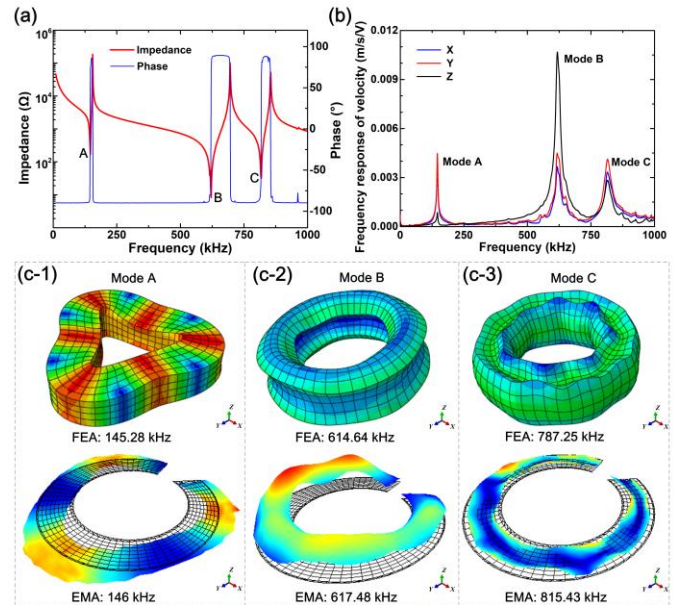
Fig. 1. (a) Electrical impedance and phase characteristics of the piezoelectric ring. (b) Frequency response of the average velocity on the surface of the piezoelectric ring per unit voltage. (c) FEA and EMA results of the piezoelectric ring showing three vibration modes, Mode A, Mode B and Mode C, from 10 kHz to 1 MHz.

Coefficient values for electromechanical characteristics of the piezoelectric ring for mode A, B and C are further compared in Table 1. The effective electromechanical coupling coefficient, k_{eff}, was calculated from the impedance spectrum data using equation $k_{eff}^2 = (f_a^2 - f_r^2)/f_a^2$, where f_a is the

anti-resonance frequency and f_r is the resonance frequency [18], providing a measurement of the electromechanical conversion efficiency. The mechanical Q factor was estimated for different resonances from the impedance spectrum data. As shown in Table 1, the resonance frequencies agree well between the impedance measurements and EMA experiments. Also, Mode B (the thickness mode) exhibits the largest electromechanical coupling coefficient (k_{eff}), the lowest impedance value (Z_{min}) and the highest mechanical Q, confirming the feasibility of employing the thickness mode of the piezoelectric ring to design the ultrasonic micro-hole craniotomy device.

TABLE 1
ELECTROMECHANICAL CHARACTERISTICS OF THE PIEZOELECTRIC RING

	Mode A	Mode B	Mode C
f_r(Impedance) [kHz]	146.0	620.9	818.3
f_r(EMA) [kHz]	146.0	617.49	815.43
f_a [kHz]	155.3	695.4	855.6
k_{eff}	0.341	0.450	0.292
Z_{min}[Ω]	169.1	8.21	31.8
Q	143.3	460.0	285.1

B. Device Design and development

The ultrasonic micro-hole craniotomy device was designed based on the configuration of a Bolt Langevin Transducer (BLT). As shown in Fig. 2(a), a stack of 4 piezoelectric rings were sandwiched between a cylindrical back mass and a step shape front mass. The perforator tip with a terminal diameter of 500 μm was attached to the front mass. Regarding the materials, titanium alloy (Ti-6Al4V) was used for the micro-hole perforator, including the front mass, the back mass and the perforator tip; A4 tool steel was used for the pre-stress bolt and copper was used for the electrodes (Table 2). Mimicking the acupuncture needle, a 60° conical tip was designed at the end of the perforator tip. Fig. 2(b) shows a miniaturized ultrasonic micro-hole craniotomy prototype device in comparison with a pen. This perforator was tuned to its 1st longitudinal mode (L1) at a resonance frequency close to 22.5 kHz.

TABLE 2
MATERIAL PROPERTIES FOR COMPONENTS OF THE MICRO-HOLE CRANIOTOMY DEVICE

	Ti6Al4V	A4 tool steel	Copper
Density ρ [kg/m^3]	4430	8000	8900
Young's modulus E [GPa]	109	210	110
Poisson's ratio v	0.313	0.29	0.37
Acoustic impedance [Pa.s/m×10^6]	27.32	45.40	41.61

To understand vibrational behaviors of the miniaturized micro-hole perforator in Fig. 2(a-b), FEA and EMA experiments were performed. To assist displacement amplitude measurement, a 500 μm diameter tool with a blunt tip was used as it was difficult to stably attach a laser reflective tape on a conical tip. As shown in Fig. 2(c-d), there is a good agreement between the vibration mode shape predicted by FEA and the EMA measurement. The longitudinal displacement node was found to locate at the flange; the amplification gain showed a consistent value around 5.4 (defined as the ratio of the

amplitude at the perforator tip to the amplitude at back mass's end surface), indicating that ultrasonic vibration generated by the piezoelectric rings could be amplified by 5.4 times to achieve a large amplitude at the tip.

Table 3 further compares the electromechanical characteristics of the miniaturized micro-hole craniotomy device from FEA or EMA measurements. Resonance frequency f_r of the L1 mode predicted by FEA was similar to that measured in EMA, with a difference smaller than 2.6%; the amplification gain from FEA or EMA also showed a constant value of 5.3 to 5.4. Results in Fig. 2 and Table 3 show that we have established a reliable framework for the design and fabrication of the miniaturized ultrasonic micro-hole craniotomy device.
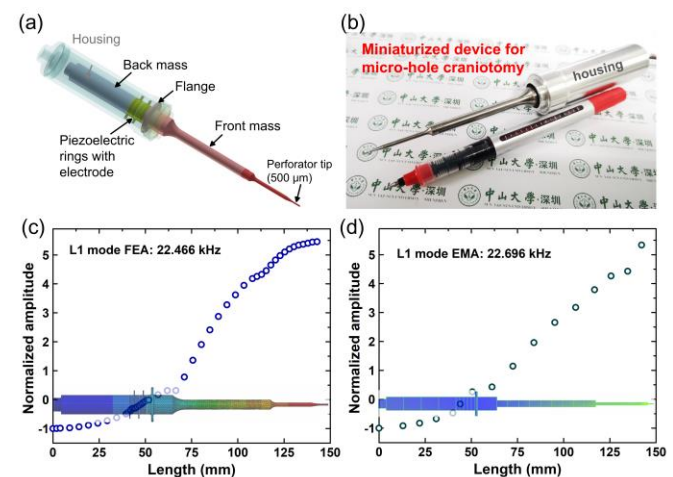
Fig. 2. The miniaturized ultrasonic micro-hole craniotomy device. (a) The 3D model. (b) The miniaturized miniaturized ultrasonic micro-hole craniotomy device in comparison with a pen. (c) FEA results showing the vibration mode shape of the L1 mode. (d) EMA results showing the vibration mode shape of the L1 mode.

TABLE 3
ELECTROMECHANICAL CHARACTERISTICS OF THE ULTRASONIC TOOL

f_r (FEA) [kHz]	22.47
f_r (Impedance) [kHz]	23.06
f_r (EMA) [kHz]	22.7
f_a (Impedance) [kHz]	23.41
k_{eff}	0.712
Z_{min} [Ω]	702.7
Q	213.6
Amplification gain (FEA)	5.45
Amplification gain (EMA)	5.33

C. Characterization of Device Performance

To ensure optimal vibration, effects of pre-stress applied on piezoelectric rings on vibration behaviors were investigated by incrementally increasing the torque. As shown in Fig. 3(a-b), the change in resonance and anti-resonance frequencies diminished as the tightening torque was increased (see Fig. 3(a) for impedance-frequency curves under different press-stress torques). At a torque of 3.0 Nm, there was no evident increase in the resonance and anti-resonance frequencies. The ultrasonic device with a press-stress torque of 3.0 Nm was further left for 5 days, allowing the piezoelectric rings to age.

Harmonic analysis experiments were performed to study the vibration responses of the ultrasonic device excited in resonance (L1 mode) at escalated high excitation levels for practical use. Excitation was applied around the resonance frequency of the L1 mode with a burst sine signal generated by a signal generator (Agilent 33210A, Santa Clara, CA, USA) and amplified by a power amplifier (HFVA-62, Nanjing Foneng Technology Industry Ltd, Nanjing, China). Longitudinal vibration response was measured using a 1D laser Doppler vibrometer (OFV 303, Polytec GmbH, Waldbronn, Germany) from a grid point on the front face of the perforator tip. To minimize frequency shifts caused by heating of piezoelectric rings at high excitation levels, each sine burst signal had 5000 oscillation cycles, which was sufficient to ensure a steady state while minimizing thermal effect. Also, a 2-second interval was applied between sequential bursts to ensure a constant temperature for a complete frequency sweep. The displacement amplitude-frequency responses were measured at different levels of excitation voltage.

Fig. 3(c-d) shows a maximal frequency shift of around 200 Hz at an excitation voltage of 60 V_{rms}. This nonlinear dynamic behavior could be exacerbated when the ultrasonic tool is engaged with the bone material due to the "vibro-impact" response between the perforator tip and the external load [19]. As shown in Fig. 3(c), the amplitude increased at a higher excitation level. A zero-to-peak amplitude of 27 µm was achieved at a voltage 60 V_{rms}. Also, the amplitude-frequency curves demonstrated a "softening" nonlinear response [20], with the backbone bending to the left. At a voltage higher than 20 V_{rms}, the "jump" phenomenon occurred, which would be due to the loss in piezoelectric properties at escalated excitations [21].

To deal with the nonlinear vibration responses in Fig. 3(c-d), a robust resonance tracking system based on auto-resonance control strategy is required to maintain the working efficiency of the ultrasonic device for high quality micro-hole generation on skull [22]. In this study, the resonance tracking system PDUS210 FLEX (Piezodrive) for real-time resonance tracking during skull perforation was employed. The resonance tracking unit is based on the auto-resonance control [23], which consists of a positive feedback loop [21], locking the phase of the applied AC voltage and current to ensure maximal energy transfer; a negative feedback control loop is also implemented to maintain a prescribed electrical current level by automatically adjusting the input voltage, which can indirectly help maintain the desired ultrasonic vibration amplitude.

Fig. 3(e) shows the electrical impedance of the miniaturized micro-hole perforator measured by the PDUS210 FLEX unit. The impedance magnitude is around 686.5 Ω at a resonance frequency of 23.26 kHz, demonstrating a good match with the impedance measured by the impedance analyzer. Further, the relationship between the prescribed electrical current and the vibration amplitude at the tip of the perforator was characterized by a 1D laser Doppler vibrometer (LDV). As shown in Fig. 3(f), a linear trend existed between the driving current and the vibration amplitude, with a peak-to-peak amplitude of 44.6 µm at a driving current of 0.15 A. By adjusting the driving current, vibration amplitude of the

ultrasonic tool could be conveniently controlled for micro-hole craniotomy.
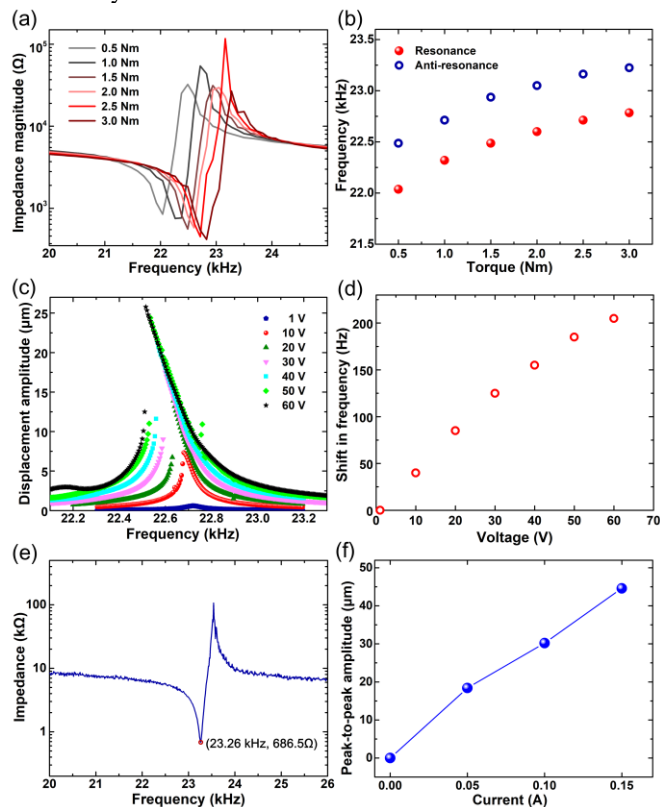
Fig. 3. (a) The L1 mode impedance-frequency spectrum of the developed ultrasonic micro-hole craniotomy device with increasing torques. (b) Effects of tightening torque on resonance and anti-resonance frequencies. (c) Vibration-frequency characteristics of the device at different excitation voltages. (d) Shift in resonance frequency as a function of excitation voltage. (e) The impedance-frequency response of the ultrasonic device measured by Piezodrive. (f) Relationship between the vibration amplitude (peak-to-peak) and the driving current.

Thus, through rational design with FEA analysis and EMA characterization, we successfully designed a miniaturized ultrasonic micro-hole craniotomy device with a resonance frequency around 23 kHz and a maximal peak-to-peak amplitude of 44.6 µm. In the following, high quality micro-holes generation on skull without material removal will be investigated with this miniaturized ultrasonic micro-hole craniotomy device.

D. Experiment conditions and sample preparation

The experiment setup for micro-hole perforation on skull is shown in Fig. 4(a). The developed ultrasonic device with a 60° conical tip (diameter: 500 µm; Fig. 4(b)) driven by the PDUS210 FLEX was used for micro-hole perforation in *vitro* on rabbit skull. The ultrasonic device was mounted on a micro-precision 3-axis translational stage. Bone sample was clamped by a sample holder which was mounted on a force sensor (LH-SZ-60F3; capacity: 49.0 N). Micro-hole perforation process was monitored with a CCD camera; the thrust force was recorded by a data acquisition device (USB 6218, National

Instruments, Austin, TX, USA). Skull bone samples were harvested from adult New Zealand rabbits (18-21 weeks) with institutional approval (Institutional Animal Care and Use Committee approval No.: SYSU-IACUC-2022-000621). Rabbits were sacrificed by injecting overdose pentobarbital sodium. Samples were harvested from the central part of skull to reduce variation in sample thickness. Harvested bone samples were measured to have an average thickness of 1.54 ± 0.26 mm (n = 5). Before experiment, bone samples were preserved in the physiological saline solution to keep them hydrated.
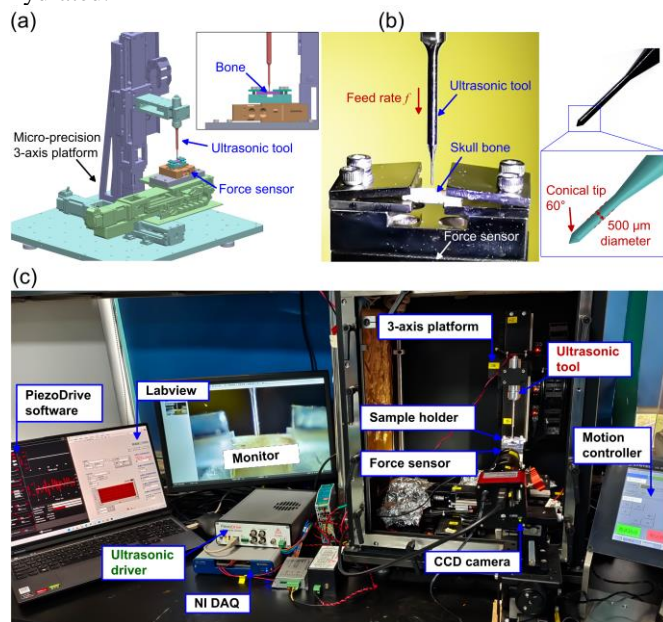
Fig. 4. (a) 3D model of the experiment setup for micro-hole perforation tests. (b) Zoom-in view of the ultrasonic micro-hole craniotomy device feeding towards the skull bone. (c) The experiment platform for in vitro micro-hole craniotomy tests on skull bone samples.

Effects of vibration amplitude on micro-hole perforation were investigated at three different amplitudes with a constant feed rate of 0.05 mm/s. Vibration amplitude was varied by adjusting the current value of the ultrasonic driver (see Fig. 3(f)). Feed rate was also varied to study the effect on micro-hole perforation. Thrust forces for micro-hole perforation under different vibration amplitudes and feed rates were recorded and compared. After micro-hole perforation, bone samples were dried, sputter-coated with gold and observed under scanning electron microscope (SEM) to measure hole diameter and characterize surface morphology of micro-holes generated under different conditions. For accurate measurement of the hole diameter, bone samples were polished with sandpapers to prepare a flat surface for micro-hole generation. Bone samples were also cleaved to expose the inner surface of micro-holes for surface morphology characterization.

III. RESULTS AND DISCUSSION

A. Micro-hole generation on skull with an extremely small force

Fig. 5(a) shows representative force curves for skull penetration by the ultrasonic micro-hole craniotomy device at different vibration amplitudes; skull penetration without ultrasonic vibration was used as control. As skull bone has a typical three-layer structure (the outer layer and the inner layer being the cortical bone and the inner layer being the sponge bone), two peaks can be detected on force curves, with the first and the second peak indicating the penetration of outer and inner cortical bone, respectively. Without ultrasonic vibration, although the micro-tool could penetrate skull bone in some cases, an extremely large force (peak force > 35 N) was experienced by the micro-tool; after penetration, a large residual force (> 10 N) still persisted, which would be attributed to friction between the elastically deformed bone tissue and the micro-perforator. Also, as the surface of skull bone was not ideally flat, a large lateral force could be introduced in the initial indentation stage, which caused tool bending and fracture sometimes in the experiment, making the non-ultrasonic micro-hole perforation unsafe for clinical use. With the introduction of ultrasonic vibration, the thrust force was greatly reduced, as observed in the ultrasonic vibration assisted bone drilling [8, 24, 25]. Upon skull penetration, the thrust force reduced to zero, showing that the micro-hole perforation process could be accurately controlled with close-loop force-displacement control.

Fig. 5(b) further compares the maximum thrust force required for micro-hole perforation on skull at different amplitudes (n = 6; feed rate: 0.05 mm/s). In the control case (non-ultrasonic vibration), an average thrust force of 20.7 ± 2.9 N was needed for skull penetration. Low amplitude ultrasonic vibration (peak-to-peak amplitude: 18.4 μm) reduced the maximum thrust force to 16.3 ± 3.6 N, which was further reduced to 3.6 ± 2.2 at an amplitude of 30.2 μm. At the largest amplitude of 44.6 μm, an extremely small force of 0.98 ± 0.67 N was observed, which would enable safe micro-hole perforation on skull without tool fracture.

In the micro-hole perforation process, the apparent ultimate stress σ_u experienced by skull bone at amplitudes of 0 μm, 18.4 μm, 30.2 μm and 44.6 μm were 105.5 MPa, 83.1 MPa, 18.3 MPa and 5.0 MPa, respectively. Linearly fitting the data, we have $\sigma_u = \sigma_0 - 2.46A$, where A is the vibration amplitude and σ_0 is the nominal ultimate strength of the skull bone used in this study. σ_0 (110 MPa) estimated here is of the same order of magnitude as reported in the literature [7, 17]. Findings in Fig. 5(b) imply that with the assistance of large amplitude ultrasonic vibration, the skull bone could be penetrated at a considerably small nominal stress.

Fig. 5(c) further compares the maximum thrust force for micro-hole perforation on skull under different feed rates at a constant amplitude of 44.6 μm (peak-to-peak). The feed rate was found to have a great influence on the thrust force. When the feed rate was increased to 0.50 mm/s, the thrust force soared to 21.2 ± 11.5 N, which was about 22 times higher than that at a feed rate of 0.05 mm/s. Similar observations were reported in

the drilling of composite materials [26]. In the micro-hole perforation process, bone tissue below the ultrasonic tool would go through microscopic fracture and plastic deformation due to the high frequency hammering of the conically tipped tool. At a higher feed rate, there would be less time for the ultrasonic tool to squeeze bone tissue aside; bone tissue accumulated below the micro-perforator would present more resistance to the micro-tool, leading to a larger thrust force as experimentally observed [26, 27]. Findings in Fig. 5(b-c) show that with the assistance of high amplitude ultrasonic vibration at a low feed rate, the high strength skull bone can be easily penetrated by the ultrasonic micro-hole perforator with a force smaller than 1 N, which has not been achieved before to the best of our knowledge.
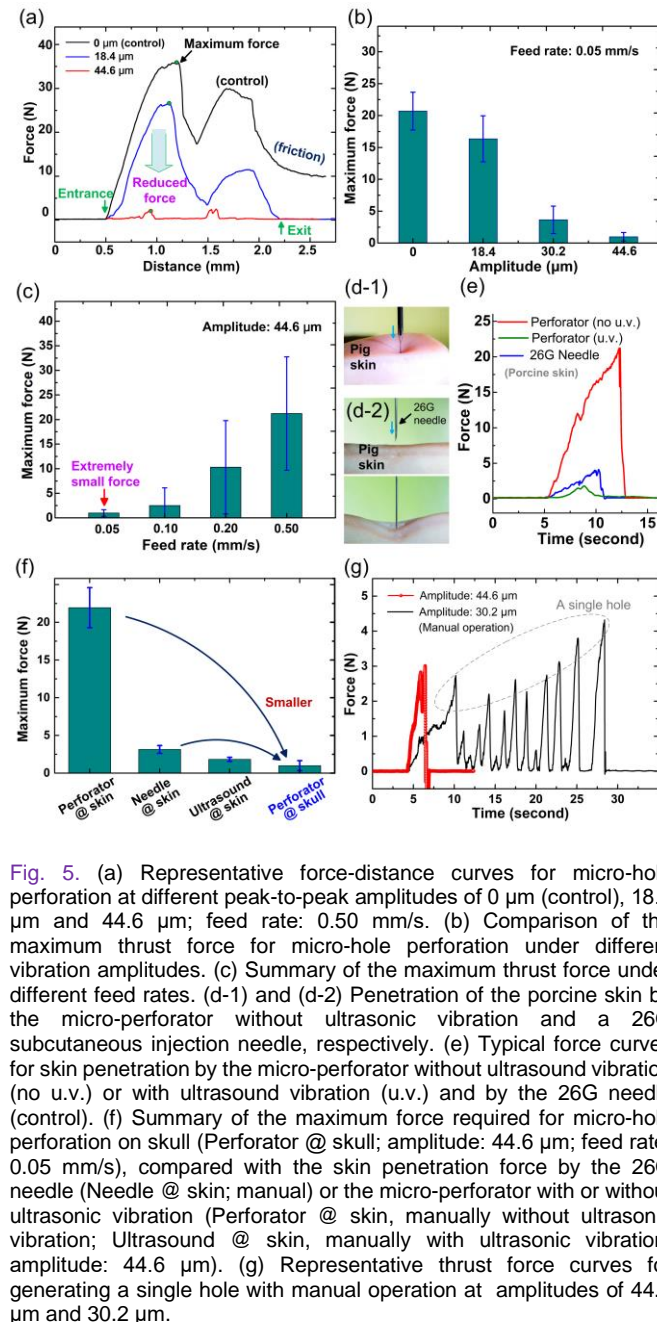
Fig. 5. (a) Representative force-distance curves for micro-hole perforation at different peak-to-peak amplitudes of 0 μm (control), 18.4 μm and 44.6 μm; feed rate: 0.50 mm/s. (b) Comparison of the maximum thrust force for micro-hole perforation under different vibration amplitudes. (c) Summary of the maximum thrust force under different feed rates. (d-1) and (d-2) Penetration of the porcine skin by the micro-perforator without ultrasonic vibration and a 26G subcutaneous injection needle, respectively. (e) Typical force curves for skin penetration by the micro-perforator without ultrasound vibration (no u.v.) or with ultrasound vibration (u.v.) and by the 26G needle (control). (f) Summary of the maximum force required for micro-hole perforation on skull (Perforator @ skull; amplitude: 44.6 μm; feed rate: 0.05 mm/s), compared with the skin penetration force by the 26G needle (Needle @ skin; manual) or the micro-perforator with or without ultrasonic vibration (Perforator @ skin, manually without ultrasonic vibration; Ultrasound @ skin, manually with ultrasonic vibration, amplitude: 44.6 μm). (g) Representative thrust force curves for generating a single hole with manual operation at amplitudes of 44.6 μm and 30.2 μm.

To highlight this outstanding performance, ultrasonic vibration assisted micro-hole perforation on skull was compared to skin penetration by a sharp needle. Skin penetration tests were performed with the same micro-hole perforator (without ultrasonic vibration) and a 26G needle with a sharp bevel tip that was clinically used for subcutaneous injection (outer diameter: 450 μm). Before experiment, the porcine skin was covered with a cotton gauze saturated with phosphate buffered saline solution to sufficiently hydrate the skin tissue. Porcine skin was manually penetrated by the non-ultrasonic micro-perforator and the 26G needle (Fig. 5(d-1) and (d-2), with the force measured by a force sensor ($n = 6$, Fig. 5(e-1)).

Fig. 5(e-2) compares the maximum force required for the micro-perforator to penetrate porcine skin (Perforator @ skin; without ultrasonic vibration) or the skull bone (Perforator @ skull; with ultrasonic vibration), compared with the skin penetration force by the 26G needle (Needle @ skin; control). In the control group (26G needle), despite the sharp tip, an average force of 3.14 ± 0.52 N was experienced by the 450 μm diameter subcutaneous injection needle. As for the micro-perforator, its tip was not as sharp as the 26G needle, leading to an unexpectedly large force of 21.94 ± 2.66 N during skin penetration; with ultrasonic vibration, the maximum penetration force reduced to 1.83 ± 0.27 N (Ultrasound @ skin, Fig. 5(e-2)), possibly due to the cavitation effect during skin penetration. Compared with the force for penetrating soft skin by the sharp subcutaneous injection needle, the force required for ultrasonic vibration assisted micro-hole formation on skull was 68.8% smaller (amplitude: 44.6 μm; feed rate: 0.05 mm/s). We thus provide an effective method for micro-hole perforation on the hard skull with a force (< 1 N) even smaller than that for subcutaneous injection on soft skin. In the next stage, intelligent control algorithm will be developed based on the force-displacement curve in Fig. 5(a) for accurate end-point detection during micro-hole perforation on skull.

In practical application, it is challenging to manually maintain a stable and consistent feed rate. To test the effects of manual operation on thrust force, micro-hole perforation was manually performed at vibration amplitudes of 44.6 μm and 30.2 μm (see representative thrust force curves during manual operation in Fig. 5(g)). Manual operation was found to generate a thrust force of 3.79 ± 0.60 N ($n = 5$) at the amplitude of 44.6 μm, which was significantly larger than that performed with numerically control at a feed rate of 0.05 mm/s (0.98 N, Fig. 5(b)). At a smaller amplitude of 30.2 μm, the thrust force increased to 4.08 ± 0.40 N ($n = 5$), which would be owing to the tool-bone interaction of reduced intensity. Besides, as reflected from the force curve in Fig. 5(g), manual perforation at the amplitude of 30.2 μm was halted a few times in order to prevent damage to the micro-perforator. Therefore, to ensure low force micro-hole perforation on skull, the miniaturized micro-hole perforator can be operated by a robotic arm.

Meanwhile, at the end of skull penetration, tip of the ultrasonic tool would inevitably contact dura mater, a tough membrane beneath skull composed of fibroblasts and extracellular collagen. In vitro experiments were performed to

clarify if contact between the ultrasonic tool and dura would instantly damage or penetrate the dura. Dura mater harvested from the New Zealand rabbit was clamped by the sample holder (Fig. 6(a)); the ultrasonic tool (vibration amplitude: 44.6 μm) was feed towards the dura mater at a feed rate of 0.05 mm/s. As shown in Fig. 6(b), the ultrasonic tool did not damage or penetrate the soft dura mater after contact. With the advancement of the ultrasonic tool, the dura mater was deformed and bulged without breaking. After about 44 seconds' sustained contact, the dura mater started to be penetrated by the tip of the micro-tool as reflected from the force-displacement curve in Fig. 6(c), due to the excessive deformation of the dura mater at the contact point (bulging height: ~2.2 mm; see the bottom-right image in Fig. 6(b)).

Results in Fig. 6(b-c) reveal that at the end of skull perforation, contact of the dura mater by the ultrasonic tool would not damage or penetrate the soft dura mater. This would be owing to the frequency designed for the ultrasonic tool (~23 kHz) in the current study. Ultrasonic tools with frequency blow 30 kHz can selectively fragment hard bone tissue without causing damage to adjacent soft tissue [28], like the commercial Piezosurgery® device used in maxillofacial or spine surgery [29, 30].
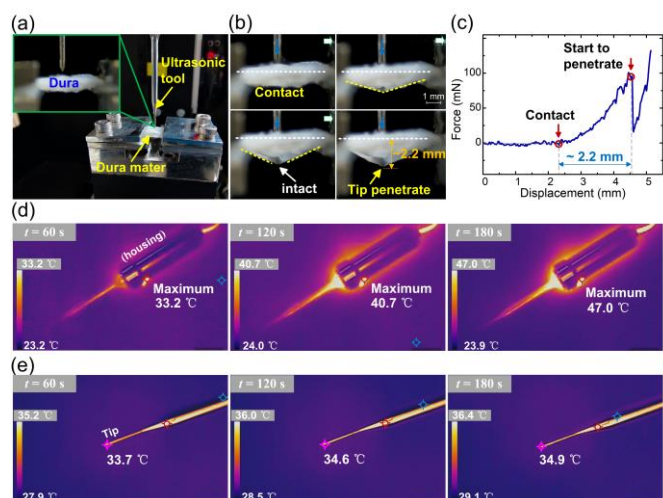
Fig. 6. (a) The setup for in vitro tool-dura interaction tests. (b) Deformation of the dura mater by the ultrasonic tool; vibration amplitude: 44.6 μm; feed rate: 0.05 mm/s. (c) A representative force-displacement curve of the dura mater with the advancement of the ultrasonic tool; tool-dura contact did not instantly cut or penetrate the dura mater, the dura was bulged and eventually penetrated due to large deformation. (d) Maximum temperature measured at device's housing and (e) its tip after 3 minutes' operation.

Besides, temperature profile of the ultrasonic device during operation was also investigated with an infrared camera (K20, HIKMICRO ltd.; room temperature: 24 ℃) [31]. Temperature was measured after 180 seconds' operation, which would be enough for human skull perforation even at a low feed rate of 0.05 mm/s (human skull thickness ranges from 2 to 8 mm [32]). As shown in Fig. 6(d-e), after 3 minutes' operation, the maximum temperature at the housing (near to the transducer) increased to 47 °C (Fig. 6(d)), while the temperature at the tip of

the tool was only 34.9 °C (Fig. 6(e)) which would not cause necrosis to bone tissue or soft tissue [31, 33]. Similar to commercial ultrasonic bone scalpels, if cooling system were integrated into the ultrasonic device and physiological coolant were used during micro-hole perforation [29, 30], thermal effect to bone tissue or soft tissue could be further minimized for micro-hole generation on skull.

B. Precision of micro-hole perforation on skull

The micro-hole generated on skull is intended to be used as a guide hole for minimally invasive insertion of micro-tools in brain for targeted diagnostic or treatment purpose. Elastic recovery of deformed bone tissue may change the hole diameter after tool withdraw. To investigate this effect, micro-holes generated at different vibration amplitudes were observed under SEM to measure hole diameter ($n = 4$).

Fig. 7 compares the diameter of micro-holes generated at different amplitudes and feed rates. As shown in Fig. 7(a), at a low vibration amplitude, micro-holes appeared to have a smaller diameter. For instance, micro-holes generated at the amplitude of 18.4 μm had a diameter of 438.1 ± 17.2 μm, much smaller than that of the micro-hole perforator (diameter: 500 μm). Low intensity tool-bone tissue interaction at a decreased amplitude would lead to insufficient plastic deformation to bone tissue; elastic recovery after tool retrieval would make the hole have a smaller diameter than that of the micro-tool. At an increased amplitude of 30.2 μm, the micro-hole presented a diameter of 506.8 ± 20.6 μm, which was similar to that of the micro-hole perforator; this implied that sufficient plastic deformation was achieved which effectively refrained elastic recovery and generated a hole with nearly the same diameter as the micro-perforator. However, at a the largest amplitude of 44.6 μm, micro-holes were found to have a diameter of 550.3 ± 30.1 μm, slightly larger than that of the micro-tool, which could be attributed to the undesired lateral vibration of micro-perforator's tip at a high excitation level [34]. Owing to the slender geometry of the miniaturized tool (Fig. 2(a-b), the distal tip was prone to develop lateral vibration in response to loading with high excitation, which could be mitigated by optimizing the design.
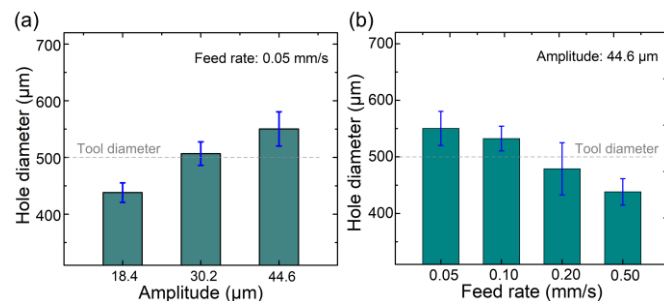
Fig. 7. Diameter of micro-holes generated at different (a) vibration amplitudes and (b) feed rates.

Similar to the vibration amplitude, the feed rate was found to have a prominent influence on hole diameter. As shown in Fig. 7(b), micro-holes were found to have a smaller diameter at a higher feed rate. At an elevated feed rate of 0.20 mm/s,

diameter of the micro-hole decreased to 478.8 ± 46.1 µm, smaller than that of the micro-tool. When the feed rate was further increased to 0.5 mm/s, micro-holes were measured a small diameter of 438.1 ± 23.3 µm, even with a large vibration amplitude of 44.6 µm.

C. High quality micro-hole formation on skull

For in-depth investigation of micro-hole perforation assisted by ultrasonic vibration, surface morphology of micro-holes generated at different vibration amplitudes and feed rates was characterized under SEM. Fig. 8 compares surface morphology of micro-holes generated under different vibration amplitudes. In the control case (without ultrasonic vibration), although the micro-tool could penetrate bone tissue sometimes free of bending or fracture, micro-holes were found to have deteriorated quality with a small diameter; layers of bone tissue residuals were observed on the inner surface of micro-hole after tool withdraw (Fig. 8(a)). In the skull penetration process without ultrasonic vibration, bone tissue was locally fractured and squeezed aside by the conically tipped tool. However, the low intensity tool-tissue interaction in the control case was not able to induce sufficient plastic deformation to bone tissue around the hole. After tool withdraw, elastic recovery of bone tissue would lead to a smaller hole diameter and formation of laminated bone tissue around the hole as observed in Fig. 8(a).

With the presence of ultrasonic vibration, high quality micro-holes were generated (Fig. 8(c)), surface morphology of the generated micro-holes was different from the control case. As shown in Fig. 8(c) and Fig. 9(a), at a high vibration amplitude of 30.2 µm, a high quality micro-hole was successfully formed with an integral edge and a smooth inner surface free of micro-cracks. At a lower vibration amplitude of 18.4 µm, although micro-holes with relatively smaller diameter and coarse edge were generated (Fig. 8(b)), no laminated bone tissue was observed on micro-hole's inner surface.

In the ultrasonic vibration assisted micro-hole generation process, the relative velocity between the micro-perforator and bone tissue can be described by $v(t) = v_0 + 2\pi f A \cos(2\pi f t)$, where v_0 is the feed rate, A is the vibration amplitude and f is the resonance frequency. For amplitude (peak-to-peak) from 18.4 µm to 44.6 µm, the maximum instant impacting speed can reach up to 1.34 ~ 3.26 m/s. As skull bone is a composite material composed of inorganic minerals and organic collagen with micro-porosities, in response to the high-intensity tool-bone interaction, this porous architecture would be locally damaged by the conically tipped ultrasonic micro-perforator, generating a micro-hole in skull bone. The high frequency hammering would plastically deform and squeeze bone tissue around the conical tip in a manner similar to ultrasonic micro-forging [35, 36], forming a dense layer of bone tissue around the hole. In this process, porous structure of bone tissue around the micro-hole would be elastically compressed to accommodate plastically deformed bone tissue.
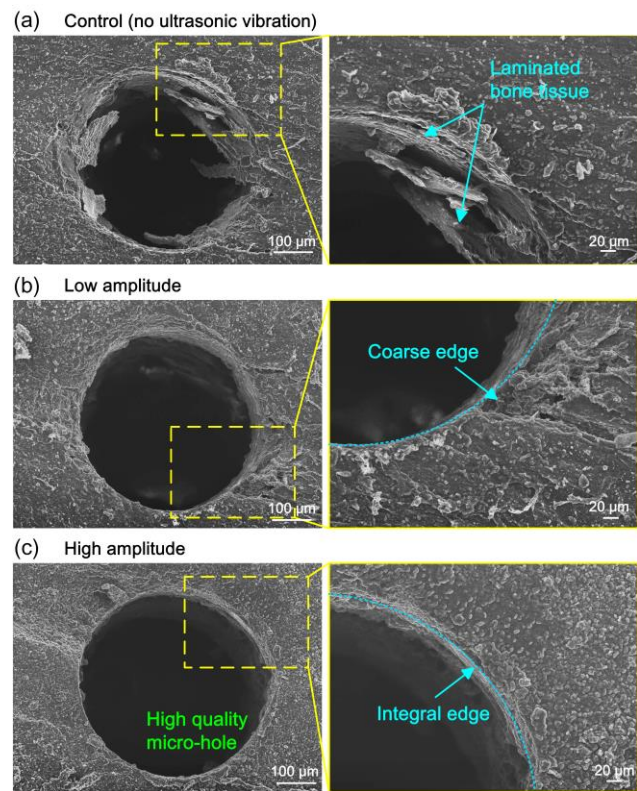
Fig. 8. SEM images showing micro-holes generated on skull at different peak-to-peak amplitudes (a) 0 µm as the control, (b) low amplitude of 18.4 µm and (c) high amplitude of 30.2 µm. Feed rate: 0.05 mm/s.

Micro-hole generation on skull assisted by ultrasonic vibration would be a balance between plastic deformation and elastic recovery of bone tissue. At a low vibration amplitude, bone tissue around the hole would be plastically deformed with a low compressive stress; elastic recovery of bone tissue after tool withdraw would lead to a micro-hole with a coarse edge and a smaller diameter as observed in Fig. 8(b). At a larger vibration amplitude, the high intensity tool-bone interaction would cause sufficient plastic deformation to bone tissue, which has refrained the elastic recovery of bone tissue after tool removal, generating a high quality micro-hole with nearly the same diameter as the micro-tool as shown in Fig. 7(a) and Fig. 8(c).

Surface morphology of micro-holes generated at different feed rates is further compared in Fig. 9 (vibration amplitude: 44.6 µm). With the increase in feed rate, the generated micro-holes showed deteriorated quality with a reduction in diameter. At a low feed rate of 0.05 mm/s, micro-holes with a clear border and a good circularity were generated (Fig. 8(c)). When the feed rate was increased to 0.10 mm/s, micro-holes with a clear border was formed; but a few subsurface micro-cracks were also observed around the hole (Fig. 10(a)), which would be attributed to the mild elastic recovery of bone tissue after tool removal. With a further increase in feed rate to 0.20 mm/s, micro-cracks and wrinkles were developed on the inner surface of the micro-hole (Fig. 9(b)), micro-burr was also detected at the entrance (Fig. 10(b)), similar to the top burr generated in micro-end milling [37, 38]. Burr formation

became more outstanding at an even higher feed rate of 0.5 mm/s, resulting in micro-holes with irregular geometry as shown in Fig. 10(c), which could not be used as the entrance hole for micro-tool insertion in minimally invasive neural intervention.
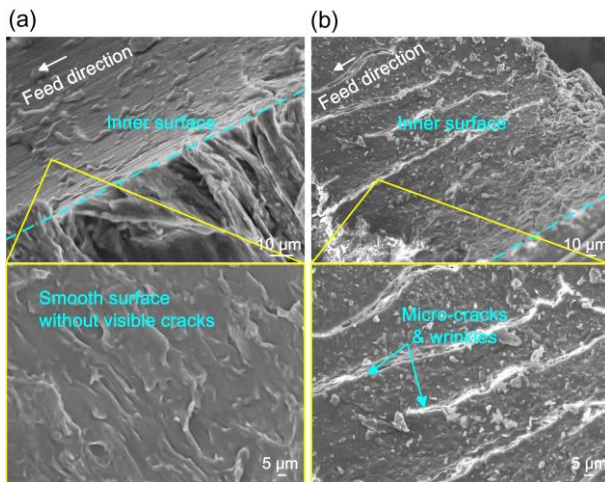
Fig. 9. SEM images of the inner surface of micro-holes generated at (a) feed rate 0.05 mm/s, amplitude 30.2 μm and (b) feed rate 0.20 mm/s, amplitude 44.6 μm.

Micro-holes generated with manual operation were also characterized under SEM (Fig. 10(d-e)). Manual operation was found to generate a micro-hole of a larger diameter (564.7 ± 16.9 μm at amplitude of 30.2 μm; 553.7 ± 36.7 μm at amplitude of 44.6 μm; $n = 3$), which would be due to tool tilting or shaking during manual operation. Also, different from the micro-holes generated with numerical control (Fig. 8(b-c)), manually generated micro-holes were observed to have deteriorated quality. Powdery bone debris were observed around the hole (Fig. 10(d-e)), implying that manual holding caused ejection of fractured bone particles in the hole forming process; unstable manual operation also lead to micro-holes with enlarged entrance as observed in Fig. 10(d). Besides, at a smaller amplitude (30.2 μm), manual operation would lead to micro-holes of irregular geometry, with burr formed at the entrance and laminated bone tissue formed on the inner surface (Fig. 10(e)). Thus, for precise and high quality micro-hole generation, numerical controlled operation would be preferred.

Deteriorated hole quality at elevated feed rate would be related to the following two factors: firstly, the duration of tool-bone interaction (or cycles of ultrasonic hammering per depth) at an increased feed rate would be significantly reduced, resulting in insufficient plastic deformation of bone tissue around the hole. Secondly, skull bone was reported to have a larger elastic modulus at a higher strain rate [39, 40]; bone tissue would stiffen at a higher feed rate, making it more challenging for the micro-tool to deform the bone tissue as revealed from the increase thrust force at higher feed rates in Fig. 5(c). Thus, for high quality micro-hole generation on skull, a relatively smaller feed rate (such as ≤ 0.1 mm/s) would be desired to facilitate sufficient plastic deformation on bone tissue around the micro-hole. Considering the fact that human

skull has an average thickness of about 6-7 mm [7], it would take about 1~2 minutes for the micro-hole perforation on skull with the method/device developed in this study at a feed rate of 0.05 ~ 0.1 mm/s. Compared with the conventional burr hole drilling technique, this method would be quick enough to facilitate minimally invasive neural intervention.
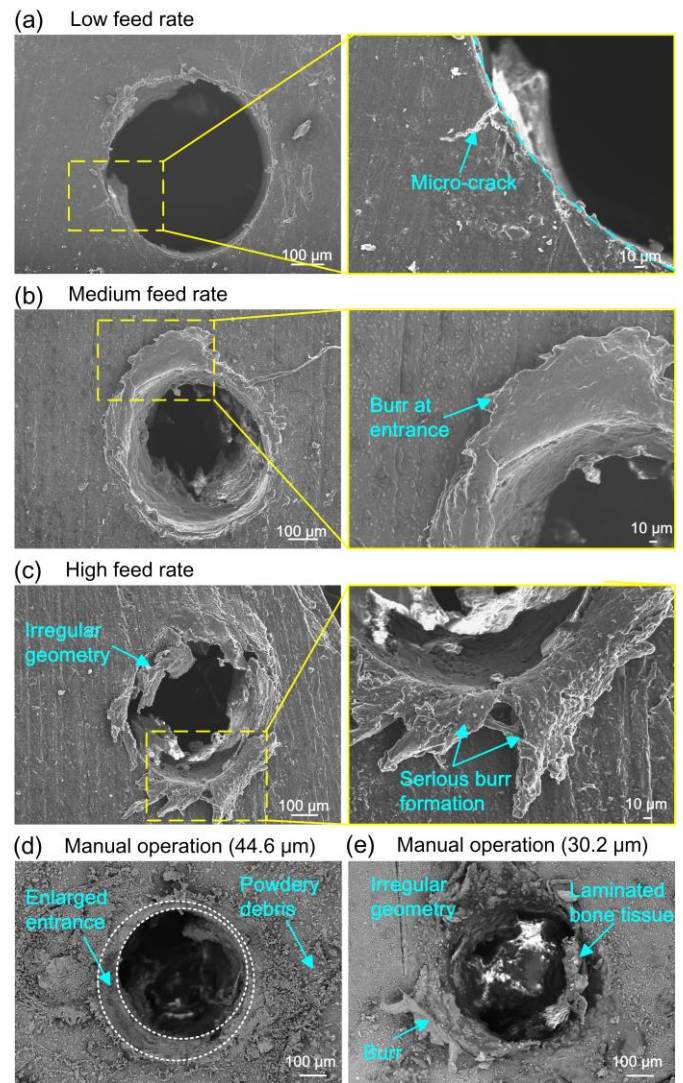
Fig. 10. SEM images of micro-holes generated on skull bone at different feed rates: (a) 0.10 mm/s, (b) 0.20 mm/s, (c) 0.50 mm/s, (d) manual operation at a peak-to-peak amplitude of 44.6 μm, and (e) manual operation at the amplitude of 30.2 μm.

Based on the above investigations, we have shown that with the miniaturized ultrasonic micro-hole perforator, high quality micro-holes can be generated on hard skull with the assistance of high amplitude ultrasonic vibration at an extremely small force, which will provide a safe and effective method for micro-hole perforation on skull. Different from micro-hole drilling or grinding where tissue cutting/removal is involved, micro-hole perforation on skull is implemented with a novel mechanism without material removal, similar to subcutaneous injection. Taking advantages of skull bone's unique material

properties (especially its porous structure), an ultrasonic micro-hole perforator can locally damage and plastically deform bone tissue for micro-hole craniotomy on skull. Micro-hole formation characteristics are affected by displacement amplitude and feed rate of the device, which could take effect by influencing the intensity and duration of tool-bone interaction. Under optimized conditions (large displacement amplitude and low feed rate), high quality micro-holes could be easily formed on the hard skull bone with a force even smaller than that for subcutaneous injection on skin (soft tissue).

Compared with the conventional bone micro-drilling, micro-hole perforation on skull could be achieved by the ultrasonic device with a force smaller than 1 N; in contrast, the maximum thrust force for micro-hole drilling on bone would be up to 4 N as previously reported [41], which would significantly increase the risk of drill bit fracture. Also, as the micro-hole is formed without material removal, the micro-hole generated on skull could be clearly visualized and accessed by micro-catheters or micro-electrodes for neural intervention; in contrast, bone chips generated during bone drilling would accumulate around the micro-hole, which needs to be carefully cleaned after surgery [41, 42]; otherwise, powdery bone debris/chips may partially block the micro-hole, impairing subsequent neural intervention.

Therefore, with the miniaturized micro-hole perforator, this study has presented a method for micro-hole perforation on the high strength skull bone (a bio-composite material with micro-porosities) without material removal. Integrating the miniaturized micro-perforator with a robotic arm, it is anticipated that minimally invasive neural intervention can be implemented through a micro-hole on skull in a minimally invasive manner similar to subcutaneous injection or acupuncture [1-3, 43]. Another advantage of this method is that unlike the conventional large burr hole drilling, micro-hole perforation proposed in this study would cause neglectable damage to the skull; after neural operation, the micro-hole could be easily sealed with a plaster, significantly promoting post-operation recovery.

IV. CONCLUSION

In this article, a novel method for micro-craniotomy on skull has been presented, which can be performed in a minimally manner similar to subcutaneous injection or acupuncture on soft tissue. For this purpose, a miniaturized ultrasonic micro-hole perforator device was developed with rational deign and systematic characterization. In-depth investigation of the micro-hole craniotomy mechanism was performed with systematic experiments on animal skull. Effects of vibration amplitude and feed rate on micro-hole forming characteristics including thrust force, diameter and morphology of generated micro-holes were systematically investigated. Exploiting skull bone's unique structural and material properties, the ultrasonic micro-perforator could locally damage the bone tissue with micro-porosities and induce sufficient plastic deformation to the bone tissue around the micro-hole and refrain elastic recovery after tool withdraw, thus providing a novel method for micro-hole generation on skull without material removal. Under optimized conditions, it is shown that a high quality micro-hole could be generated on the hard skull with a force (< 1 N) even smaller than that for subcutaneous injection on soft skin. With the minimally invasive micro-hole perforation technique and the miniaturized ultrasonic tool developed in this study, we anticipate that neural operations such as localized drug delivery, neural sensing, tissue biopsy or tumor treatment can be implemented in a manner similar to subcutaneous injection through a micro-hole on skull, bringing great benefits to both patients and the research community.

REFERENCES

[1] R. Qazi *et al.*, "Wireless optofluidic brain probes for chronic neuropharmacology and photostimulation," *Nat. Biomed. Eng.*, vol. 3, no. 8, pp. 655-669, Aug. 2019.

[2] K. B. Ramadi *et al.*, "Focal, remote-controlled, chronic chemical modulation of brain microstructures," *Proc. Nat.l Acad. Sci. USA*, vol. 115, no. 28, pp. 7254-7259, Jul. 2018.

[3] C. Dagdeviren *et al.*, "Miniaturized neural system for chronic, local intracerebral drug delivery," *Sci. Transl. Med.*, vol. 10, no. 425, Jan. 2018.

[4] S. I. Pekov *et al.*, "Rapid estimation of tumor cell percentage in brain tissue biopsy samples using inline cartridge extraction mass spectrometry," *Anal. Bioanal. Chem.,* vol. 413, no. 11, pp. 2913-2922, May 2021.

[5] A. Niesche *et al.*, "Smart bioimpedance-controlled craniotomy: concept and first experiments," *Proc. Inst. Mech. Eng. H*, vol. 231, no. 7, pp. 673-680, Jul. 2017.

[6] H. Huiyu   *et al.*, "Investigating bone chip formation in craniotomy," *Proc. Inst. Mech. Eng. H*, vol. 231, no. 10, pp. 959-974, Oct. 2017.

[7] A. Auperrin *et al.*, "Geometrical and material parameters to assess the macroscopic mechanical behaviour of fresh cranial bone samples," *J. Biomech.*, vol. 47, no. 5, pp. 1180-1185, Mar. 2014.

[8] K. Alam *et al.*, Experimental study on the effect of point angle on force and temperature in ultrasonically assisted bone drilling," *J. Med. Biol. Eng.*, vol. 38, no. 2, pp. 236-243, Apr. 2018.

[9] S. Li *et al.*, "Information feedback self-adaptive harmony search algorithm for the bovine cortical bone vibration-assisted drilling optimization," *Measurement*, vol. 149, pp. 107020, Jan. 2020.

[10] Y. Song *et al.*, "Real-time spectral response guided smart femtosecond laser bone drilling," *Opt. Laser. Eng.*, vol. 128, pp. 106017, May 2020.

[11] K.-H. Kim *et al.*, "Effect of laser pre-drilling on insertion torque of orthodontic miniscrews: a preliminary study," JDR., vol. 10, no. 2, pp. 66-73, 2017.

[12] F. Aljekhedab *et al.*, "Influence of environmental conditions in bovine bone ablation by ultrafast laser," *J. Biophotonics*, vol. 12, no. 6, pp. e201800293, Jun. 2019.

[13] M. E. Ivan *et al.*, "Brain shift during bur hole-based procedures using interventional MRI," *J. Neurosurg.*, vol. 121, no. 1, pp. 149-60, Jul. 2014.

[14] Z. Li *et al.*, "Review on factors affecting targeting accuracy of deep brain stimulation electrode implantation between 2001 and 2015," *Stereotact. Funct. Neurosurg.*, vol. 94, no. 6, pp. 351-362, 2016.

[15] A. D. Brown *et al.*, "Shear behavior of human skull bones," *J. Mech. Behav. Biomed. Mater.*, vol. 116, pp. 104343, Apr. 2021.

[16] Q. Wu *et al.*, "Computational studies of pPorous head protection structures for human cranium under impact loading," *Acta. Mech. Solid.a Sin.*, vol. 34, no. 4, pp. 477-493, Aug. 2021.

[17] Z. Li *et al.*, "Ultrasonic vibration-assisted micro-hole forming on skull," *Proc. Inst. Mech. Eng. B J. Eng. Manuf.,* vol. 231, no. 14, pp. 2447-2457, 2015.

[18] A. Caronti, R. Carotenuto, and M. Pappalardo, "Electromechanical coupling factor of capacitive micromachined ultrasonic transducers," *J. Acoust. Soc. Am.*, vol. 113, no. 1, pp. 279-288, Jan. 2003.

[19] V. K. Astashev, and V. I. Babitsky, "Ultrasonic cutting as a nonlinear (vibro-impact) process," *Ultrasonics*, vol. 36, no.1, pp. 89-96, Feb.1998.

[20] A. Mathieson *et al.*, "Understanding nonlinear vibration behaviours in high-power ultrasonic surgical devices," *Proc. R. Soc. A*, vol. 471, pp. 20140906-20140906, Feb. 2015.

[21] Sokolov, and V. Babitsky, "Phase control of self-sustained vibration," *J. Sound Vib.,* vol. 248, pp. 725-744, Dec. 2001.

[22] X. Li *et al.*, "Experimental analysis on autoresonant control of ultrasonically assisted drilling," *Mechatronics,* vol. 29, pp. 57-66, Aug. 2015.

[23] V. I. Babitsky *et al.*, "Autoresonant control of nonlinear mode in ultrasonic transducer for machining applications," *Ultrasonics*, vol. 42, no. 1, pp. 29-35, Apr. 2004.

[24] X. Bai *et al.*, "Analysis of machining process and thermal conditions during vibration-assisted cortical bone drilling based on generated bone chip morphologies," *Med. Eng. Phys.*, vol. 83, pp. 73-81, Sep. 2020.

[25] Alam *et al.*, "Experimental investigations of forces and torque in conventional and ultrasonically-assisted drilling of cortical bone," *Med. Eng. Phys.*, vol. 33, no. 2, pp. 234-9, Mar. 2011.

[26] A. A. A. Nasir *et al.*, "Critical thrust force and critical feed rate in drilling flax fibre composites: a comparative study of various thrust force models," *Compos. Part B-eng.*, vol. 165, pp. 222-232, May 2019.

[27] U. A. Khashaba, and A. A. El-Keran, "Drilling analysis of thin woven glass-fiber reinforced epoxy composites," *J. Mater. Process Tech.*, vol. 249, pp. 415-425, Nov. 2017.

[28] M. Schlee *et al.*, "Piezosurgery: basics and possibilities," *Implant Dent.*, vol. 15, no. 4, pp. 334-40, Dec. 2006.

[29] G. Pavlikova *et al.*, "Piezosurgery in oral and maxillofacial surgery," *Int. J. Oral Maxillofac. Surg.*, vol. 40, no. 5, pp. 451-7, May 2011.

[30] A. Franzini *et al.*, "Piezoelectric surgery for dorsal spine," *World Neurosurg.*, vol. 114, pp. 58-62, Jun. 2018.

[31] E. Shakouri *et al.*, "An in vitro study of bone drilling: infrared thermography and evaluation of thermal changes of bone and drill bit," *Phys. Eng. Sci. Med.*, vol. 43, no. 1, pp. 247-257, Mar. 2020.

[32] S. H. Tretbar *et al.*, "Accuracy of ultrasound measurements for skull bone thickness using coded signals," *IEEE Trans. Biomed. Eng.*, vol. 56, no. 3, pp. 733-40, Mar. 2009.

[33] M. F. A. Akhbar, and A. R. Yusoff, "Fast & injurious: reducing thermal osteonecrosis regions in the drilling of human bone with multi-objective optimization," *Measurement,* vol. 152, pp. 107385, Feb. 2020.

[34] K.-L. Kuo, "Design of rotary ultrasonic milling tool using FEM simulation," *J. Mater. Process. Tech.*, vol. 201, no. 1, pp. 48-52, May 2008.

[35] X. Chang *et al.*, "Microforging technique for fabrication of spherical lens array mold," *Int. J. Adv. Manuf. Technol.*, vol. 96, no. 9, pp. 3843-3850, Jun. 2018.

[36] Xu *et al.*, "Ultrasonic micro-forging post-treatment assisted laser directed energy deposition approach to manufacture high-strength Hastelloy X superalloy," *J. Mater. Process. Tech.,* vol. 299, pp. 117324, Jan. 2022.

[37] R. Lekkala *et al.*, "Characterization and modeling of burr formation in micro-end milling, " *Precis. Eng.*, vol. 35, no.4, pp. 625-637, Oct. 2011.

[38] S. Y. Jin *et al.*, "Burr formation and its treatments-a review," *Int. J. Adv. Manuf. Technol.*, vol. 107, no. 5, pp. 2189-2210, Mar. 2020.

[39] J. A. Motherway *et al.*, "The mechanical properties of cranial bone: the effect of loading rate and cranial sampling position," *J. Biomech.*, vol. 42, no. 13, pp. 2129-2135, Sep. 2009.

[40] C. Santiuste *et al.*, "The influence of anisotropy in numerical modeling of orthogonal cutting of cortical bone," *Compos. Struct.*, vol. 116, pp. 423-431, Sep. 2014.

[41] Z. Liao, and D. A. Axinte, "On monitoring chip formation, penetration depth and cutting malfunctions in bone micro-drilling via acoustic emission," *J. Mater. Process. Tech.,* vol. 229, pp. 82-93, Mar. 2016.

[42] Ghanbari *et al.*, "Craniobot: a computer numerical controlled robot for cranial microsurgeries," *Sci. Rep.*, vol. 9, no. 1, pp. 1023, Jan. 2019.

[43] R. S. Zoll *et al.*, "MEMS-actuated carbon fiber microelectrode for neural recording," *IEEE Trans. Nanobioscience*, vol. 18, no. 2, pp. 234-239, Apr. 2019.